Polar surface energies of iono-covalent materials: Implications of a charge transfer model tested on Li_2FeSiO_4 surfaces

Nicolas G. Hörmann[1, 2] and Axel Groß[1, 2]

[1] *Helmholtz Institute Ulm (HIU) Electrochemical Energy Storage, Albert-Einstein-Allee 11, 89069 Ulm*
[2] *Universität Ulm, Institut für Theoretische Chemie, Albert-Einstein-Allee 11, 89069 Ulm*

(Dated: February 8, 2014)

Ionic compounds that are often used as electrode materials in Li-based rechargeable batteries can exhibit *polar* surfaces which are generally accepted to exhibit rather large surface energies. We derive an analytical estimate for the surface energy of such *polar* surfaces assuming charge redistribution as polarity compensating mechanism. The *polar* contribution to the converged surface energy is found to be proportional to the bandgap times the surface charge necessary to compensate for the depolarization field and some higher order correction terms that depend on the specific surface. Other features such as convergence behavior coincide with published results. General conclusions are drawn on how to perform *polar* surface energy calculations in slab configuration and upper boundaries of "purely" *polar* surface energies are estimated. Furthermore we compare these findings with results obtained in a DFT study of Li_2FeSiO_4 surfaces. We show that typical *polar* features are observed and provide a decomposition of surface energies into polar and local bond-cutting contributions for 29 different surfaces. We show that the model is able to explain subtle differences of GGA and GGA+U surface energy calculations.

Keywords: Computational chemistry, electrochemistry, energy storage, surface structure, ionic compounds

I. INTRODUCTION

Ionic oxide compounds are often used as electrode materials in Li-based rechargeable batteries [1]. In many ionic materials, stable crystal and surface structures and equilibrium crystal shapes can be well understood with the simple but powerful *ionic model* [2]. Still, the peculiar convergence properties for the infinite sum of long-range $\frac{1}{r}$ Coulomb potentials in fact already indicate that problems might arise for surface energy calculations, as it is especially the variability in surface contributions that lead to conditional convergence properties of Madelung-like sums and require adequate summation techniques [3, 4]. Surprisingly, basic features that are predicted within the ionic model obviously agree well with the observed trends in nature, as for example cohesive energies of alkali-halides [2].

The ionic model can also be helpful for understanding surface energy trends in ionic materials. As these often exhibit close-packed structures with non-directional bonds, their relaxation behavior at surfaces is rather small [5], at least for non-polar surfaces. Thus the energy cost of surface creation is often well represented by just looking at the differences in electrostatic energy of the surfaces as cut from the bulk crystal. As far as the classification of *polar* and *non-polar* surfaces is concerned, often a scheme according to Tasker has been used which, however, is only applicable to simple e.g. binary and ternary materials [6]. The original and more general definition was given by Bertaut [7] in 1958. He proofed most generally that any slab with non-vanishing perpendicular component of electric dipole calculated within the ionic model would have infinite surface energy. The macroscopic field leads to a constant shift in energy per unit cell with respect to bulk and hence there is a contribution to the surface energy that linearly scales with the slab thickness. It corresponds in value to the energy increase due to the depolarization field caused by the sudden truncation of the lattice. This is especially puzzling as one might speculate about the difference of an infinitely thick slab and an infinitely extended solid. Consequently *polar* surfaces are often assumed to be unstable in nature.

Drawbacks of the ionic model are the arbitrary decomposition of the continuous charge density on separate ionic cores [8, 9] which obviously leads to ambiguity in the definition of *polar* surfaces. The statement that any surface with non-vanishing dipole has infinite surface energy does not appeal to physical common sense. It implies that any surface with the smallest dipole in the repetitive unit cell, deviating by $\epsilon > 0$ from the value 0, is classified *polar* and thus unstable. Yet, some clarification has been achieved recently [10]. *Polar* surfaces do indeed exist in nature with surface energies that are unexpectedly moderate [11–13].

Several mechanisms have been proposed that stabilize *polar* surfaces such as vacancies, adatoms, reconstruction or simply charge redistributions between the surface layers [14–21]. However, we have not yet found a concise proposal on how to estimate the energy cost of any of these mechanism in a quick and general manner prior to expensive first-principles calculation. Such an estimate seems helpful for understanding the relative effectiveness of the different possible contributions and for a pre-screening of possible mechanism before performing computationally expensive calculations. Having an approximate expression for the surface energy contribution due to charge redistribution is particularly important in order to estimate and understand the surface energies of ionovalent materials which are of interest as electrode material in electrochemical energy storage.

In the first part of this paper, we derive a very simple extension to the description of *polar* surfaces and the electrostatic contribution to the surface energy within the ionic model that allows for charge redistribution in the surface region of the material. In fact, basic findings will turn out to correspond to already published considerations [20, 22], but in contrast to previous works our results are derived from a minimum energy principle. In addition, we hope to add further understanding to *polar* surface energies also in complex materials as we can derive the formulas without, e.g., presuming lattice geometry or restricting ourselves to binary or ternary materials. This enables us to draw general conclusions on upper boundaries of *polar* surface energies, convergence behavior and relevance of convergence. It might also shed light on estimation of errors e.g. in high-throughput ab-initio surface energy calculations where detailed convergence studies are rendered impossible.

In the second part we address ab-initio slab calculations based on density functional theory (DFT) which are in general well-suited to reproduce materials properties [23, 24]. We show that several predictions of our simple model manifest themselves in the iono-covalent material Li_2FeSiO_4. This material is especially interesting as possible electrode material of future Li-ion batteries [25–32]. We use our model to estimate electrostatic contributions to *polar* surface energies in this compound. The decomposition of surface energy in local bond-cutting and long-range polar contributions provides a general explanation for observed stability trends. The scheme presented in this work had already been applied by us [33], but it had not been derived in detail yet. We will report some of previous results to illustrate the power of this approach in understanding trends observed in electronic structure calculations. In addition, by using first-principles electronic structure calculations we specifically address (001) and (010) surfaces and show that distinct properties are in very good agreement with the behavior of *polar* surfaces predicted by our simple model.

II. THEORY

A. The ionic model

In order to derive the seemingly diverging behaviour of the electrostatic contribution to the surface energy of polar surfaces, a rather heuristic approach is possible that takes correctly into account the physical origin of the divergence which is the non-vanishing macroscopic E field inside a polar slab. When neglecting relaxations, the surface energy is defined by the energetic difference between a certain slab surrounded by vacuum and the equal slab embedded in the periodic bulk [34]. In the bulk material the real local electrostatic fields are of course strongly varying on the scale of the lattice constant, however, due to the periodic boundary conditions, two equivalent positions on the two surfaces of the embedded slab unit cells need to be on the same potential. This periodic boundary condition is no longer valid in the slab, and the dominating difference in the local electric fields between a *polar* slab and a respective portion of the bulk material is a constant electric E field, the depolarization field **E** (see, e.g., Fig. 7 a below or Fig. 2 b in Ref. [35]).

E is perpendicular to the surface and is related to the z component of the polarization P_z of the slab via:

$$|\mathbf{E}(P_z)| = E(P_z) = \frac{1}{\epsilon\epsilon_0} \cdot \frac{P_z}{Ad} = \frac{1}{\epsilon\epsilon_0} \sum_{z_i \in V_0} \sigma_i \frac{z_i}{d_c} = \frac{1}{\epsilon\epsilon_0}\sigma_0 \tag{1}$$

Without loss of generality we choose the z axis perpendicular to the surface, and define d as the thickness of the slab, A is the area of the surface unit cell and the slab consists of N unit cells with thickness d_c and Volume V_0. The z component of the polarization of the slab is defined by standard electrostatics [36] and related to the charge density $\rho(\mathbf{r})$:

$$\begin{aligned} P_z &= \int_V z\rho(\mathbf{r}) \quad \mathrm{d}^3r = A \cdot N \cdot \sum_{z_i \in V_0} \sigma_i z_i \\ &= Ad \cdot \sum_{z_i \in V_0} \sigma_i \frac{z_i}{d_c} = Ad \cdot \sigma_0 \end{aligned} \tag{2}$$

σ_i denotes average charges in planes parallel to the surfaces, positioned at z_i in the slab unit cell. σ_0 as defined in eq. 2 can be viewed as an effective surface charge.

The dominant term for the surface energy of such a polar slab in a purely ionic compound is the electrostatic energy of the charge distribution $\rho(\mathbf{r})$ in the depolarization field due to the sudden truncation of the crystal. It is in good approximation independent of $\mathbf{r}$ [37].

Thus the total electrostatic energy difference per area Γ due to the surface can be estimated by integration:

$$\begin{aligned} \Gamma(P_z) &= \int_0^{P_z} \frac{E(P_z')}{A} \mathrm{d}P_z' \\ &= \frac{1}{2\epsilon\epsilon_0} \cdot \left(\sum_{z_i \in V_0} \sigma_i \frac{z_i}{d_c} \right)^2 \cdot d = \frac{1}{2\epsilon\epsilon_0}\sigma_0^2 d \end{aligned} \tag{3}$$

This rather heuristic approach gives exactly the result obtained by Bertaut [7]. Obviously the surface energy will diverge proportional to d if $\sigma_0 \neq 0$. In reality however the interplay of various mechanisms will keep Γ finite, as will be addressed below.

B. The ionic model with possible charge transfer

One major mechanism of polarity compensation is a charge transfer of $\delta\sigma$ from one surface of the slab to the other which reduces the effective **E** field inside the slab to $E(P_z, \delta\sigma) = \frac{1}{\epsilon\epsilon_0} \cdot \frac{P_z}{Ad} - \frac{1}{\epsilon\epsilon_0} \cdot \delta\sigma = \frac{1}{\epsilon\epsilon_0}(\sigma_0 - \delta\sigma)$ and might correspond to surface metallization. This is equal to introducing a fictitious plate capacitor with charge

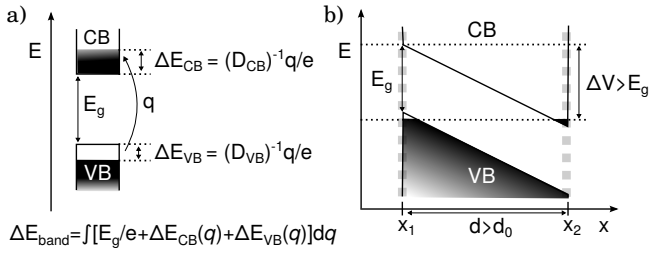

Figure 1. a) Band energy cost for redistribution of electrons from anions (valence band) to cations (conduction band). b) Local density of states bending due to the linear potential drop inside a *polar* slab. Charge transfer can only take place when the potential drop is larger than E_g/e.

$\pm\delta\sigma$ to the picture. The total electrostatic energy $\mathcal{E}$ is obtained by integration of:

$$\begin{aligned} &\mathrm{d}\mathcal{E}(P_z, \delta\sigma) = \\ &= \underbrace{\frac{1}{\epsilon\epsilon_0}\left[\frac{P_z}{Ad} - \delta\sigma\right]\mathrm{d}P_z}_{\text{slab}} - \underbrace{\frac{Ad}{\epsilon\epsilon_0}\left[\frac{P_z}{Ad} - \delta\sigma\right]\mathrm{d}\delta\sigma}_{\text{plate capacitor}} \\ &= \frac{1}{\epsilon\epsilon_0}\frac{P_z}{Ad}\cdot\mathrm{d}P_z + \frac{Ad}{\epsilon\epsilon_0}\delta\sigma\cdot\mathrm{d}\delta\sigma - \frac{1}{\epsilon\epsilon_0}\cdot\mathrm{d}(P_z\delta\sigma) \end{aligned} \quad (4)$$

Then the total energy per area $\Gamma(P_z, \delta\sigma)$ is:

$$\begin{aligned} \Gamma(P_z, \delta\sigma) &= \frac{\int \mathrm{d}\mathcal{E}(P_z, \delta\sigma)}{A} = \\ &\underbrace{=}_{\text{eq. 2}} \frac{1}{2\epsilon\epsilon_0}\left(\sigma_0^2 + \delta\sigma^2 - 2\sigma_0\delta\sigma\right)\cdot d \\ &= \frac{1}{2\epsilon\epsilon_0}\left(\sigma_0 - \delta\sigma\right)^2\cdot d \end{aligned} \quad (5)$$

Thus Γ equals the energy of a plate capacitor with reduced effective surface charge $\sigma' = \sigma_0 - \delta\sigma$. What has however been left out of the picture up to now is the electronic band energy increase due to the redistribution of $\delta\sigma$. In the bulk ionic crystal, valence and conduction band (VB and CB, respectively) are separated by the finite band gap E_g and thus charge redistribution causes a significant change of the electronic energy (see Fig. 1a).

Taking band filling effects into account, the differential electronic energy change is:

$$\mathrm{d}\mathcal{E}_{el}(\delta\sigma) = \left[\frac{E_g}{e} + \left(\frac{A}{eD_{VB}} + \frac{A}{eD_{CB}}\right)\frac{\delta\sigma}{e}\right]A\cdot\mathrm{d}\delta\sigma \quad (6)$$

where e is the charge of an electron, $\frac{D_{VB}}{A}$ and $\frac{D_{CB}}{A}$ are the VB and CB density of states (DOS) per surface area, which is taken to be constant upon band filling. They are mainly determined by the local DOS (LDOS) of surface anions (VB) and cations (CB) between which the charge transfer takes place (see Fig. 1a). If one thinks in a local charge transfer instead of a band structure picture, one might regard this effect as introducing chemical hardness or adding on-site Coulomb repulsion terms for strongly correlated materials. Effectively, any picture should lead to a similar expression as this represents a kind of Taylor expansion of the electronic energy due to charge transfer. The total energy per area including the electronic contributions reads then:

$$\begin{aligned} \Gamma_{tot}(d, \sigma_0, \delta\sigma) &= \frac{\mathcal{E} + \mathcal{E}_{el}}{A} \\ &= \frac{1}{2\epsilon\epsilon_0}\left(\sigma_0 - \delta\sigma\right)^2\cdot d + E_G|\delta\sigma| + \frac{1}{2}C\delta\sigma^2 \end{aligned} \quad (7)$$

with $E_G = \frac{E_g}{e}$ and $C = \frac{A}{D_{VB}e^2} + \frac{A}{D_{CB}e^2}$. The thermodynamically most stable configuration is the minimum of eq. 7 with respect to $\delta\sigma$. The average surface energy γ_s, which takes both surfaces of the slab areas into account, and $\delta\sigma$ will depend on d. γ_s is given by

$$2\gamma_s(d, \sigma_0) = \Gamma_{tot}(d, \sigma_0) = \min_{\delta\sigma\geq 0}\left\{\Gamma_{tot}(d, \sigma_0, \delta\sigma)\right\} \quad (8)$$

Setting the partial derivative of eq. 7 equal to zero for $\delta\sigma > 0$ gives:

$$\delta\sigma = \frac{d\sigma_0 - \epsilon\epsilon_0 E_G}{d + C\epsilon\epsilon_0} \quad (9)$$

Charge transfer will only take place for slab thicknesses thicker than d_0, where d_0 is the thickness that will result in a potential drop across the slab of E_G where the conduction band (CB) minimum on the one side of the slab is aligned with the valence band (VB) maximum on the other side (see Fig. 1b)):

$$\delta\sigma > 0 \Rightarrow d > d_0 = \frac{\epsilon\epsilon_0 E_G}{\sigma_0} \quad (10)$$

Equation 10 can be reorganized:

$$\underbrace{\frac{1}{\epsilon\epsilon_0}\sigma_0\cdot d_0}_{\text{potential across slab}} = E_G \quad (11)$$

The slab thickness d in equation 9 can be substituted with the dimensionless effective thickness d' according to $d = d_0\cdot d'$ with $d' > 0$. Then $\delta\sigma$ behaves as:

$$\delta\sigma = \begin{cases} 0 & \text{for } d' \leq 1 \\ \frac{E_G\sigma_0(d'-1)}{E_G d' + C\sigma_0} & \text{for } d' > 1 \end{cases} \quad (12)$$

The transferred charge $\delta\sigma$ converges for large d' to σ_0. The *polar* energy term vanishes and the total energy increase converges to the electronic energy increase due to a charge transfer of σ_0:

$$\Gamma_{tot}^{\infty}(\sigma_0) = \lim_{d'\to\infty}\Gamma_{tot}(d', \sigma_0) = E_G\sigma_0 + \frac{1}{2}C\cdot\sigma_0^2 \quad (13)$$

The potential drop ΔV across the slab will converge to

$$\begin{aligned} \Delta V^{\infty} = \lim_{d\Rightarrow\infty}\Delta V &= \lim_{d\Rightarrow\infty}\frac{1}{\epsilon\epsilon_0}(\sigma_0 - \delta\sigma)\cdot d \\ &= C\sigma_0 + E_G \end{aligned} \quad (14)$$

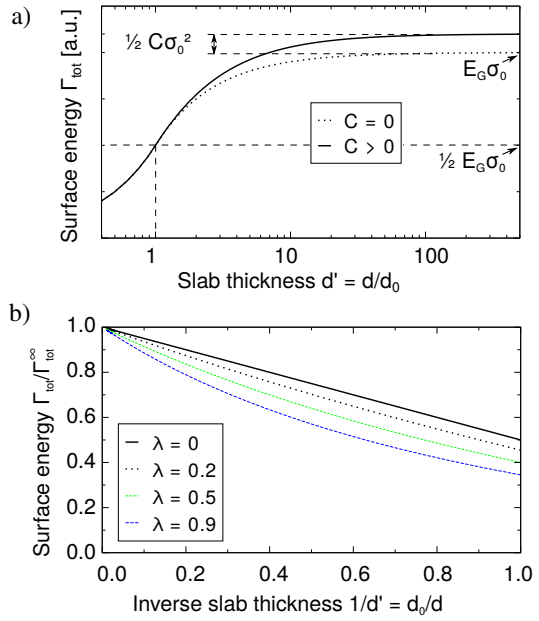

Figure 2. a) Absolute surface energy convergence of *polar* surfaces on a logarithmic thickness scale. b) Relative convergence for different band filling parameters λ on an inverse thickness scale. Thicknesses are normalized to d_0, hence are dimensionless.

This is in line with the results of Ref. [20]. $C\sigma_0$ corresponds to the additional voltage drop due to band filling. For large thicknesses, $C\sigma_O \approx E_G - \Delta V^\infty$ corresponds to the sum of the positions of the Fermi level with respect to the band edges on both sides of the slab. The total energy per area is:

$$\Gamma_{tot} = \begin{cases} \frac{1}{2} E_G \sigma_0 d' & \text{for } d' \leq 1 \\ \frac{1}{2} E_G \sigma_0 \left(\frac{\left(2 + \frac{C\sigma_0}{E_G}\right) d' - 1}{d' + \frac{C\sigma_0}{E_G}} \right) & \text{for } d' > 1 \end{cases} \tag{15}$$

Thus the surface energy increases linearly with d' as expected from the ionic model up to the point where charge transfer can take place. For large d' the total energy converges. The convergence behavior is plotted in Fig. 2 a, which is in line with results by Goniakowski *et al.* [22].

The relative convergence $\Gamma_{tot}(d')/\Gamma_{tot}^\infty$ is for $d' > 1$

$$\frac{\Gamma_{tot}(d')}{\Gamma_{tot}^\infty} = 1 - \frac{\lambda + \frac{1}{2+\lambda}}{d' + \lambda} \qquad \text{with } \lambda = \frac{C\sigma_0}{E_G} \tag{16}$$

λ is dimensionless and is just a measure for the importance of band filling. Equation 16 is plotted in Fig. 2b as a function of $1/d' = d_0/d$ for several realistic values of λ, a parameter often neglected [16, 17]. Using the definition of λ, the limiting value of Γ_{tot}^∞ (Eq. 13) can be re-expressed as

$$\Gamma_{tot}^\infty(\sigma_0) = E_G \sigma_0 \, (1 + 0.5\lambda) \, , \tag{17}$$

and the convergence behavior can be determined by expanding in orders of $\frac{1}{d'}$:

$$\begin{aligned} \Gamma_{tot}(d') &= \Gamma_{tot}^\infty - \frac{1}{2} E_G \sigma_0 \left(1 + \frac{C\sigma_O}{E_G}\right)^2 \frac{1}{d'} + \mathcal{O}\left(\frac{1}{d'^2}\right) \\ &= \Gamma_{tot}^\infty - \frac{\epsilon\epsilon_0 E_G^2}{2} (1+\lambda)^2 \frac{1}{d} + \mathcal{O}\left(\frac{1}{d^2}\right) \end{aligned} \tag{18}$$

This is the same result as in Refs. [16, 20], where, however, the correction term $C\sigma_O$ (respectively λ) is lacking.

C. Implications

C, σ_0 and ϵ are the only parameters that depend on the surface orientation (hkl). Neglecting their influence, an estimation of the surface energy can be performed solely with pure bulk parameters using eqs. 13 or 17. Of course, this just corresponds to one contribution to the total surface energy, namely due to polarity compensation. Still, general conclusions can be drawn:

1. Polar surfaces have finite surface energies and converge with increasing slab thickness according to eq. 15, in agreement with previous derivations [20].

2. If band filling effects are assumed to be small, the converged value of the *polar* contribution to surface energy is in the order of $\frac{1}{2} E_G \sigma_0$. Thus large band gap materials have energetically more costly *polar* surfaces. Furthermore, *polar* surface energies are expected to be proportional to σ_0, i.e., to the dipole moment of the slab unit cell divided by its volume.

3. The explicit dependence on E_G indicates that a good representation of E_g is a prerequisite for accurate results in ab-initio calculations of *polar* surface energies.

4. Polar ionic surfaces have a macroscopic E-Field inside a slab of finite thickness that does not decay. Therefore it seems wrong at first sight to perform ab-initio slab calculations with only relaxing atoms near the surface. Charge compensation, however, reduces the E-Field as the effective surface charge decreases with increasing thickness d. For large d, the layer relaxation in the center of the slab will become smaller (as also discussed, e.g., in Ref. [16]). Although the critical thickness d_0 and the convergence behavior do depend on ϵ (see eqs. 10 and 18), the final surface energy does not (eq. 13))! Hence we expect no difference between *converged* results of calculations in which only near-surface atoms are allowed to relax and those in which all atoms are allowed to relax. In fact, convergence will be quicker if atoms in the center of the slab are not allowed to relax (set $\epsilon = 1$ in eqs. 10 and 18 instead of $\epsilon > 1$ when allowing ionic response in the center of the slab).

5. The static dielectric response ϵ can be determined by the convergence behaviour, or comparing the surface energies of same slabs with and without relaxed inner atoms (see section III C). λ might, however, have an influence as its value can vary from surface to surface (for example, $\lambda \approx 1 \neq 0$ can be estimated from Fig. 3 in Ref. [16]).

6. Γ_{tot}^{∞} allows to estimate the size of the converged *polar* surface energy contribution. Within this context it is also possible to define **strongly** *polar* and **weakly** *polar* surfaces. Those surfaces with relatively large effective surface charge are rather high in energy, whereas the influence of polarity on the total surface energy for those with small effective surface charge should be not too large. In other words, small surface charges can be compensated rather easily. Those *polar* surfaces should have rather small energy contributions due to polarity compensation.

7. From the behavior in Fig. 2 b the necessary thicknesses for surface energy convergence can be estimated. For reasonable values of $\lambda \in [0, 0.5]$, γ_s is converged better than 90% for thicknesses $d > 10\ d_0$. This means, if we are interested in observing any of the charging/convergence effects, necessarily the relation $d < 10\ \mathrm{d_0}$ has to hold. Hence surfaces with small dipole $\neq 0$ exhibit converged surface energies only for very large thicknesses (e.g. 100 Å)! These surfaces on the other hand will have small absolute *polar* surface energies, such that the surface energy will be probably governed by bond cutting contributions.

D. Rough estimates

With the derived equations it is possible to estimate how large the influence of *polarity* compensation on surface energies is.

- **Surface energy**: Assume for typical non-conducting materials $E_G(1 + 0.5\,\lambda) \approx 3\,\mathrm{V}$. Then, using eqs. 8 and 17, one obtains

$$\gamma_s = \frac{1}{2}\sigma_0 E_G(1 + 0.5\,\lambda) \lessapprox 1.5\,\sigma_0 \cdot \mathrm{V} \qquad (19)$$

So the surface energy is of the order of σ_0 (times one Volt for the sake of dimension). The prototypical (0001) ZnO *polar* surface has a surface charge of 0.055 e/Å^2 (assuming charges equal to oxidation state). Thus the electrostatic contribution to surface energy can be estimated to be 80 meV/Å^2 $\approx$ 1.3 J/m^2, whereas the determined surface energy is 3.4 J/m^2 [13, 17]. The contribution to the total surface energy is only to one third due to the *polarity* (see also the comparison of the ZnO (1010) and (0001) surfaces in Ref. [12]). This indicates that indeed *polar* surfaces are not at all as unstable as frequently stated and should definitely be taken into consideration if for example Wulff-shapes are determined. These values should also be compared to formation energy of steps or vacancies in order to find the favorable polarity compensation mechanism.

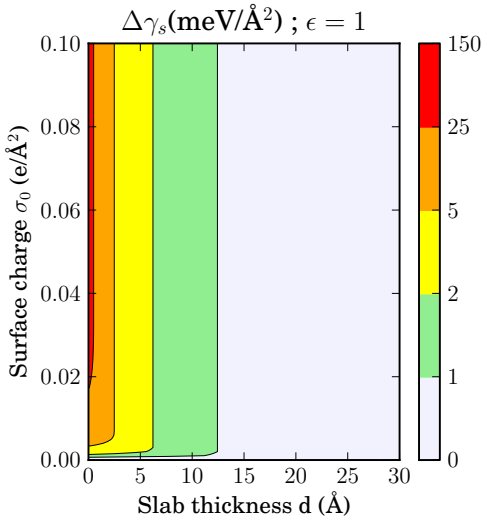

Figure 3. Contour plot of the upper bounds of the surface energy error due to finite slab thickness $\Delta\gamma_s$ with $\lambda = 0$ and $E_G = 3$ V for $\epsilon = 1$. Sufficient energy accuracy can be assumed for $\Delta\gamma_s < 1$ meV/Å^2 corresponding to the area in light grey.

- **Convergence behavior**: Assume $\lambda = 0$ and $E_G = 3\,\mathrm{V}$. Then the error in the surface energy due to the finite thickness d of the slab $\Delta\gamma_s = \gamma_s^{\infty} - \gamma_s(d)$ $d > d_0$ is according to eq. 18 approximately

$$\Delta\gamma_s = \frac{1}{2}\sigma_0 E_G \frac{\frac{1}{2}d_0}{d} = \frac{1}{4}\epsilon\epsilon_0 E_G^2 \frac{1}{d} \approx \frac{\epsilon}{d} \cdot 12.4\,\mathrm{meV/Å} \qquad (20)$$

$\Delta\gamma_s$ is essentially independent of σ_0 (see Fig. 3, where $\Delta\gamma_s$ is plotted as a function of σ_0 and d). Typical surface energies are between 20 and 100 meV/Å^2. Hence reasonable convergence should be obtained for slabs of 15 Å thickness with no relaxation of central atoms ($\epsilon = 1$). The independence on σ_0 and the absolute size indicates that indeed accurate surface energies might be obtained without performing detailed convergence studies with extrapolations to infinite thickness, when central atoms are not relaxed. As an example, we found $\epsilon \approx 2$ (see section III C), which seems reasonable as the main part of the dielectric screening is due to electronic polarization, which is also present for fixed atom coordinates, and not due to geometric relaxation.

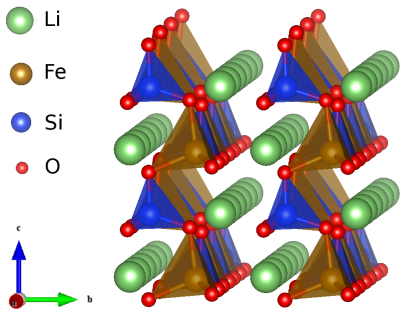

Figure 4. 2x2x2 supercell of bulk $Pmn2_1$ Li_2FeSiO_4. Colors (as in the rest of the paper): Li: *green*, Fe: *brown*, Si: *blue*, O: *red*

III. APPLICATION TO SURFACES OF $PMN2_1$ LI_2FESIO_4

Our original motivation of deriving a simple but rather general energy expression for the energy cost of polarity compensation by charge redistribution in *polar* surfaces was to understand observed trends in the calculated surface energies of $Pmn2_1$ Li_2FeSiO_4 whose bulk structure is illustrated in Fig. 4. This material is interesting for future insertion electrodes in rechargeable Li ion batteries. As the bulk unit cell has no center of inversion, there are many possible *polar* terminations.

First we present results that show that indeed also a complex material such as Li_2FeSiO_4 that consists of mainly ionic (Li-O, Fe-O) but also of mainly covalent bonds (Si-O) exhibits *polar* slab behavior that can be understood within the ionic model as explained above. Afterwards we discuss and explain the subtle differences in surface energies obtained by density functional theory (DFT) calculations using the generalized gradient approximation (GGA) for the description of the exchange-correlation effects and the so-called GGA+U exchange correlation functionals and test the predictions of our theoretical work.

A. Method

The presented results are obtained by DFT calculations using the periodic electronic structure code VASP [38, 39] with the GGA exchange-correlation functional according to Perdew, Burke and Ernzerhof (PBE) [40] and its GGA+U extension in the rotationally invariant form [41]. The effective U parameter in the +U correction scheme for the Fe 3d states was set to 4 eV, consistent with previous studies [42–44]. Dipole corrections have been applied in order to take account of the macroscopic dipole field arising from the polar nature of the surfaces. The obtained accuracy for total energies is about 2.5 meV/atom which results in final surface energy errors of approximately 2-3 %. A detailed description of the technical parameters, procedures and material properties is given in Ref. [33]. Whereas extraction voltages are found to depend strongly on the exchange correlation functional,x as expected [42, 45], the geometric properties of bulk and relaxed surface structures do not. In fact, we find small differences in surface energies for several stoichiometric terminations, consequently the influence of the particular choice of the exchange-correlation functional on the minimum energy crystal shape (Wulff shape) is negligible [33]. Apart from *non-polar* (010) and (110) terminations, the equilibrium shape of $Pmn2_1$ Li_2FeSiO_4 also exhibits *polar* (001) surface terminations which will be discussed in more detail here.

B. Bulk properties

The bulk density of states (DOS) obtained in GGA and GGA+U calculations of Li_2FeSiO_4 is shown in Fig. 5 a. There are in fact local Fe d-states in the gap which pin the Fermi energy and result in a GGA value of E_{g1} of just 0.3 eV in agreement with Ref. [46]. These are minority spin states which are the last to be filled as expected from Hund's rules for Fe^{2+} with the configuration $3d^6 = |\uparrow\downarrow|\uparrow|\uparrow|\uparrow|\uparrow|$. For delithiated $LiFeSiO_4$ (Fig. 5 b), Fe has an oxidation state of 3+ and indeed we observe that the minority spin states are emptied (note the shifted x-axis in Fig. 5 a and b). It is important to note that we find accordingly maximum integer magnetizations. In the case of the GGA+U approach we find the gap E_{g1} between filled majority and minority spins (see Fig. 5) slightly different from other publications [46, 47]. The computed DOS in Fig. 5 a and b shows that the delithiation is connected with a change of the oxidation state of the transition metal, hence in this case an emptying of the minority Fe d-levels, which become the conduction band states.

The authors of Ref. [46] find the same DOS for $LiFeSiO_4$, but a bandgap reduction upon delithiation; we, on the other hand, find an increase (when we take E_{g2} as the bandgap). This might be due to a different technical setup used in our calculations, for example a higher cutoff energy in the plane wave expansion [33]. For charge redistributions only the sum $E_{g1} + E_{g2}$ is relevant, which is in agreement with previous works. Increasing U_{eff} in the GGA+U scheme increases both values E_{g1} and E_{g2}, as illustrated in Figs. 5a and 6. Furthermore, for GGA ($U_{eff} = 0$) Fe 3d derived majority spin bands are separated by a finite energy from the O 2p derived ones. For increasing U_{eff}, however, we observe a closing of this gap and an increased mixing of Fe 3d majority states with the O 2p bands. In addition, the Fe 3d majority states are shifted to lower energies: Whereas for $U_{eff} = 2$ eV the main hybridization of Fe-d–O-p is still near the top of the VB, it shifts strongly to the bottom part for $U_{eff} = 4$ eV. This behavior is in line with the understanding of increasing U within band structure models for transition metal (TM) compound [48–50]. In fact, they describe for example a transition from Mott-Hubbard to charge-transfer

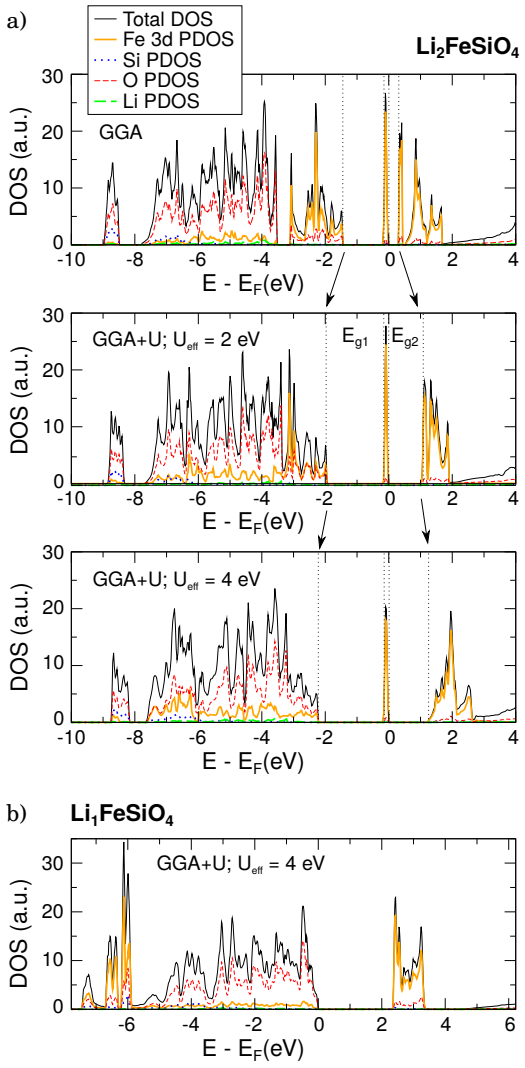

Figure 5. a) Plot of the bulk Li_2FeSiO_4 GGA (upper), GGA+U DOS for U_{eff} = 2 eV (middle) and U_{eff} = 4 eV (lower). The projections of the total DOS on Fe 3d, Si, O and Li states is drawn in different colors. b) GGA+U DOS for U_{eff} = 4 of half delithiated $LiFeSiO_4$. We set E_F to the top of the valence band as in many other publications.

insulator with increasing U and predict a linear dependence of E_g only in the Mott-Hubbard range, where the band gap is of d-d type. In this way we can understand the dependence of $E_{g1} + E_{g2}$ on U_{eff} where the majority spin d-levels move from initially above the O-2p band towards the lower part of the O-2p band, where we observe a deviation from the linear behaviour of $E_{g1} + E_{g2}$ as soon as Fe-3d and O-2p mix (at approximately 2 eV, see Figs. 5a and 6). The delithiated structure can unambiguously be classified as a charge transfer insulator, as Fe levels shift strongly to the lower end of the VB, which has strong O character at the VB maximum (see Fig. 5 b).

In any case, independent of the exchange correlation

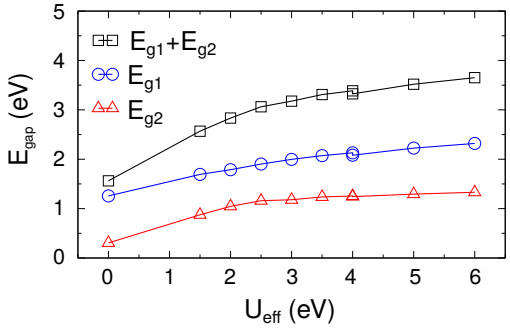

Figure 6. Band gap of bulk Li_2FeSiO_4 according to GGA+U calculations as a function of U_{eff} for the Fe 3d states.

functional, this as well as previous studies agree in the fact that Fe 3d minority levels of $Li_2Fe\ SiO_4$ lie above or at the top end of the O 2p derived band, which makes it in principle a Mott-Hubbard insulator (d-d bandgap). Hence a hole on oxygen, respectively an oxygen with reduced charge, is always less favorable than a hole in the topmost Fe d levels, i.e., an oxidized Fe^{3+}. Hence we can understand what the lowest energy charge compensation mechanism in *polar* surfaces looks like for this material: Fe atoms with different charge state on different sides of the *polar* slab. It should be mentioned that this is indeed different from normal insulators, as charge redistribution is not connected with surface metallization here, due to the local nature of Fe d states. The cost of redistributing one electron between two Fe^{2+} (the chemical hardness) which might be formally described as $2 \cdot Fe^{2+} \rightarrow Fe^{3+} + Fe^{1+}$ does not depend specifically on the position of highest Fe-d state but obviously corresponds to $E_{g1} + E_{g2}$. This should hence be the relevant "bandgap" when we apply our estimate for *polar* energies in this material.

C. The *polar* (001) surface

In Ref. [33], we report on surface energy calculations of stoichiometric surfaces of Pmn21 Li_2FeSiO_4. Indeed, typical *polar* behavior could be observed for several *polar* surfaces. As an example we will analyze the most stable stoichiometric (001) *polar* termination here. The geometry is depicted in Fig. 7c. The strong covalent bonds between Si and oxygen makes this termination indeed more stable than the less corrugated one, with the leftmost oxygen situated at its periodic image in surface 2. It resembles in geometry the widely studied (0001) termination of ZnO. The depicted termination is also *polar*, however, with a potential drop in the opposite direction.

The electronic and geometric properties of the the *polar* Pmn21 Li_2FeSiO_4 (001) slab shown in Fig. 7 were obtained using the GGA+U approach with U_{eff} = 4 eV. The ionic model suggests a positive dipole moment corresponding to a surface charge of 0.004 e/Å^2, which should be compensated by a charge transfer from surface 1 to

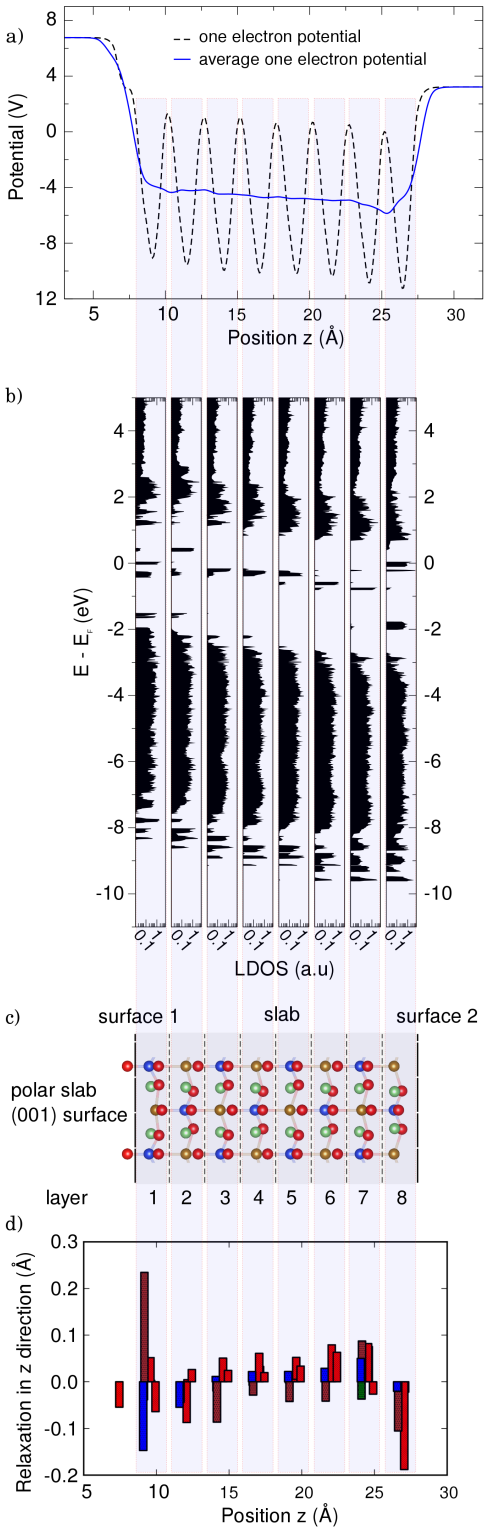

Figure 7. Properties of the prototypical *polar* Pmn21 Li_2FeSiO_4 (001) slab obtained within GGA+U. a) Electrostatic potential inside the slab. b) LDOS of the different layers. c) Geometry of the slab. d) Relaxation of atoms in the different layers (Li: *green*, Fe: *brown*, Si: *blue*, O: *red*). Plots are aligned horizontally according to the layers.

surface 2. As a matter of fact we observe such a behavior:

- The electrostatic one-electron potential is plotted in Fig. 7a (dotted line). The potential is averaged over planes perpendicular to the z axis, which is chosen perpendicular to the slab. The nearly linear drop in potential inside the slab can be seen in the blue full line corresponding to the average over a thickness of one layer.

- This is consistent with the obtained DOS that is drawn layer by layer in Fig. 7b on a logarithmic scale. Apart from the surface regions we observe a similar DOS as for bulk that shifts linearly according to the potential drop (compare this to Figs. 1b and 5). In the surface regions, especially near surface 1, we observe, however, significant deviation from the bulk DOS, which we relate to the sensitivity of the localized d levels on charge state and environment. The total potential drop across the slab is 3.5 V. As explained above the relevant bulk bandgap is $E_{g1} + E_{g2}$ for which we obtain a value of 3.4 eV (see table I). Using eq. 10 with the charge density σ_0 derived from the formal oxidation state of the surface atoms, a thickness $d_0 = 4.5$ Å results. Recall that this is the thickness at which the potential drop across the slab corresponds to the nominal band gap. This indicates that charge transfer and convergence should be achieved for the ≈ 20 Å thick slab, such that the limiting potential drop is given basically by the bandgap, as observed.

- Indeed, we also find the anticipated charge transfer between the two surfaces in this slab: Fe atoms near surface 1 are oxidized (charge reduction, increased magnetic moment), Fe atoms near surface 2 reduced (charge increase, decreased magnetic moment) (see table II).

- Furthermore, the observed potential drop inside the slab, which is connected to the depolarization field inside the slab, leads to a dielectric response of the ions, a relaxation also in the center of the slab that counteracts the perturbation, as Fig. 7d illustrates. As the material, however, consists not only of two oppositely charged sub-lattices the response is slightly more complex. We have already analyzed the relaxation in our previous paper [33], concluding that the SiO_4 tetrahedra are very rigid due to the strong and directional covalent bonds and relax rather as a single united building block of the material. Accordingly, also here, Si and O sub-lattices

Table I. E_{g1} and E_{g2} for GGA and GGA+U with $U_{eff} = 4$ eV.

GGA		GGA+U	
E_{g1} =1.26 eV	E_{g2} = 0.31 eV	E_{g1} = 2.13 eV	E_{g2} = 1.26 eV

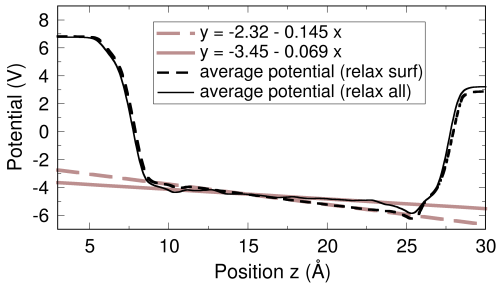

Figure 8. Electrostatic potential in the (001) *polar* slab (GGA+U) with relaxation of all atoms of the slab (thin full line) and with relaxation of only near-surface atoms (dashed line).

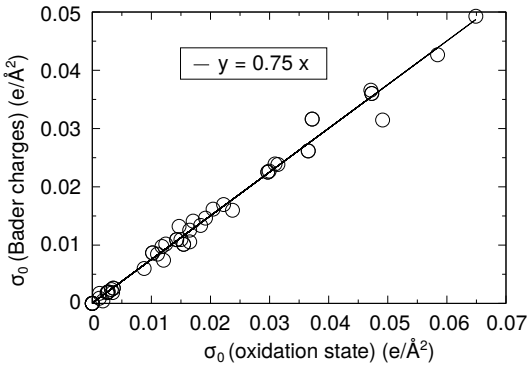

Figure 9. Bader charge σ_0^{Bader} vs oxidation state charge σ_0^{ox} for several possible surfaces in Li_2FeSiO_4. The line represents a linear fit which gives a slope of 0.75.

do not move independently from each other, but instead a concerted movement of SiO_4^{4-} subunits to the right and a corresponding movement of Fe^{2+} to the left can be observed (see Fig. 7d).

We checked whether our understanding of the dielectric response of the central atoms is correct by performing calculations, where only near-surface atoms were relaxed (up to 5 Å below the surface, i.e., layer 1 including the leftmost O and layers 7, 8). In Fig. 8 we have drawn the average one electron potentials inside the slab for the (001) slab for the two cases: in one case allowing all atoms to relax and in the other case only relaxing near-surface atoms. Obviously the former case allows for additional dielectric screening by ionic relaxation and reduces the total potential drop as well as the field inside the slab. In principle the depolarization field that is felt in the center of the slab is similar to an external field. Hence we could estimate the contribution of ionic relaxation to the dielectric constant ϵ_{ion} $(\omega = 0, q = (00\frac{1}{\infty})) \approx \frac{0.14463}{0.06873} \approx 2.1)$. We recognize that we neglect here the change in the field due to electronic redistribution in the surface region.

Nevertheless, the example shows that indeed certain typical properties of *polar* surfaces can be observed for this material and correlated to the ionic model as derived in the first part. Hence, when it comes to understanding the stability of stoichiometric surfaces it is appropriate to take *polar* contributions into account.

Table II. Local magnetic moments and charges on the Fe atoms as obtained from the projection of the charge density on Fe orbitals. Values are normalized to bulk, where we know the exact magnetization of 4 μ_b, which is related to 6 localized 3d electrons. Note the charge transfer as expected from the potential drop.

layer	1	2	3	4	5	6	7	8
Fe magnetization	4.54	4.92	4.01	4.00	4.00	3.99	3.99	2.53
electrons on Fe	5.38	5.01	5.96	5.99	5.99	6.01	5.98	7.68

D. Surface energies of Li_2FeSiO_4 surfaces

In order to pre-screen the low energy terminations of Li_2FeSiO_4, we constructed a simple model expression for surface energies in order to estimate the surface energy prior to DFT calculations [33]. We assumed that the surface energy can be approximated by the sum of local bond cutting contributions and a term due to charge redistribution in the case of *polar* slabs, as derived above:

$$\gamma_s(\lambda) = \frac{\sum_{(i,j)} E_{i,j} \cdot n_{i,j}(\lambda)}{2A(\lambda)} + K \cdot \sigma_0(\lambda) \qquad (21)$$

where $E_{i,j}$ is the energy necessary for creation of an under-coordinated surface atom of type i and coordination j, $n_{i,j}(\lambda)$ the number of these atoms for the slab with surface λ and $A(\lambda)$ the surface area. The polar surface energy contribution is estimated by $K \cdot \sigma_0(\lambda)$, where we neglect the band-filling term. For Li_2FeSiO_4, the band picture is problematic as this material rather shows a redistribution of charges among localized Fe d-states. However, as stated in the discussion of eq. 6, also a Taylor expansion of the electronic energy due to charge redistribution would lead to a term with the same functional form. For calculation of the effective surface charge density $\sigma_0(\lambda)$ we assumed formal oxidation state charges at the ion positions. A Bader charge analysis obtained from GGA bulk charge density resulted in local ionic charges as given in Tab. III.

The correlation between surface charge densities for several unreconstructed, stoichiometric *polar* slabs de-

Table III. Ionic charges in Li_2FeSiO_4 as determined by a Bader charge analysis.

element	Li	Fe	Si	O
q^{ox}/e	1	2	4	-2
q^{Bader}/e	0.85	1.27	3.11	-1.52
$q^{\text{Bader}}/q^{\text{ox}}$	0.85	0.64	0.78	0.76

rived from formal oxidation state charges (σ_0^{ox}) and from a Bader charge analysis ($\sigma_0^{\mathrm{Bader}}$) is plotted in Fig. 9. There is a good linear relationship between both approaches, where $\sigma_0^{\mathrm{Bader}} \approx 0.75\sigma_0^{\mathrm{ox}}$. Due to the simplicity of the oxidation state approach and the fact that indeed no ab-initio charge density needs to be known, σ_0^{ox} shall from now be simply referred to as σ_0. This further avoids any discussion about the appropriate approach to project the electronic charge density onto single atoms [8, 51].

Equation 21 was fitted to surface energies of 29 surfaces of $Li_2Fe\,SiO_4$, calculated within GGA. The obtained fitted parameters are given in table IV, which are discussed in detail in Ref. [33].

From the fit we obtain 0.383 V for the value of K. Considering that the real surface charge is $\sim 0.75\sigma_0$, this corresponds to a theoretical value (assuming C = 0, see eq. 19) of $E_g = e \cdot E_G = \frac{2e}{0.75}K = 1.0\,\mathrm{eV}$. The bulk GGA density of states of $Li_2Fe\,SiO_4$ suggests 1.6 eV (see Fig. 6). Hence the order of magnitude is in good agreement with the fitted value of K. We have checked the quality of the fit using different electrostatic energy expressions $K \cdot \sigma_0^n(\lambda), n \in \mathbb{N}$. Indeed we find the least residue for n = 1, and we find the fit error to be 30% smaller when including the *polar* charge compensation term "$K \cdot \sigma_0$" as compared to fitting solely with a bond-cutting expression. The root mean squared error (RMSE) of our model is 9%.

We are aware that indeed the highly correlated d states in this material questions the validity of some assumptions in the above derivation as, e.g., filling of fixed single particle states can not account for correlations in total energy or significant changes in the Hartree energy term. Nonetheless, the good quality of our parameterization indicates that the fitted value for K, which is more related to a Taylor expansion of the energy due to charge redistribution, does not necessarily have to correspond exactly to the bandgap as determined from the bulk Kohn-Sham energy eigenvalues.

A fit of eq. 21 allows to decompose the surface energy into bond cutting and electrostatic contributions in *polar* surfaces. A note of caution here: $n_{i,j}$ and σ_0 were determined from bulk properties since the derived equations are only valid for periodic systems, as is the derivation of Bertaut [7]. Therefore any relaxation related effects are included effectively in the fit parameters. The results are plotted in Fig. 10 together with the determined DFT values. The electrostatic energy contribution due to charge redistribution for polarity compensation (red) does not play a major role. The main contribution is indeed due to bond cutting. The aforementioned considerations on ZnO as well as these findings indicate that materials with mixed iono-covalent bonds seem to be mainly driven by local bond cutting and not *polarity* (see Fig. 10), a finding that seems not to have been stated clearly up to now in the literature.

Table IV. $E_{i,j}$ and K, as obtained from fitting eq. 21 to the 29 GGA surface energy values.

$E_{i,j}$ (eV)		coordination 1	2	3
element	Si	12.193	3.150	2.676
	Fe		1.835	0.712
	Li	2.361	1.147	0.398
K (V)			0.3831	

One might e.g. wonder if relaxation is driven by *polarity*. The total dipole, however, has not been found to reduce consistently upon relaxation, which corresponds to the fact that *polarity* cannot be entirely removed by surface relaxation. Obviously, surface relaxation is mainly driven by rebonding.

We are aware that GGA fails to properly describe the localized d states of TM oxides. However, when it comes to the relative stability of surfaces we observe that GGA and GGA+U are not too far apart; Wulff shapes, e.g., were found to be rather similar (see Ref. [33]). As seen in section III B, the main differences between the GGA and GGA+U DOS are basically the opening of the gap and the hybridization of O-p–Fe-d states. Of course, both will influence the surface energy: Hybridization is connected to changed Fe-O bond energies, the increased d-d gap affects charge redistribution energies. Hence it is not trivial to completely understand the differences of GGA and GGA+U calculations. We have identified one pair of surface terminations that shall be analyzed in the following which illustrates the applicability and correctness of the derived "*polar* energy" term as well as our approach to decompose the total surface energy into bond-cutting and *polar* contributions. In fact, we will take advantage of the tunability of E_g by changing U_{eff} within the GGA+U approach in order to specifically analyze the influence of the bandgap on the surface energy.

E. The *non-polar* and the *polar* (010) termination

The two (010) terminations under study are drawn in Fig. 11. The *non-polar* one corresponds to the most stable stoichiometric surface we have found for this material. Slabs are symmetric and only Li-O bonds are broken. It is, however, possible to construct an asymmetric slab by shuffling one Li atom per surface unit cell from one surface to the other at its periodic image position. The obtained slab is *polar* with a strong dipole across the slab. These two surfaces are termed (010) and (010)* in Figs. 10 and 11. In addition, the coordination of the shuffled Li atom is different for the two terminations: whereas it is doubly coordinated in the *non-polar* slab it is only singly coordinated in the *polar* slab. Hence the surface energy is much larger for the *polar* termination (see table V).

What makes this pair of terminations special is the fact that we are able to separate bond-breaking from charge-transfer effects in the surface energy and compare it to our theory. As only Li-O bond breakings are involved in

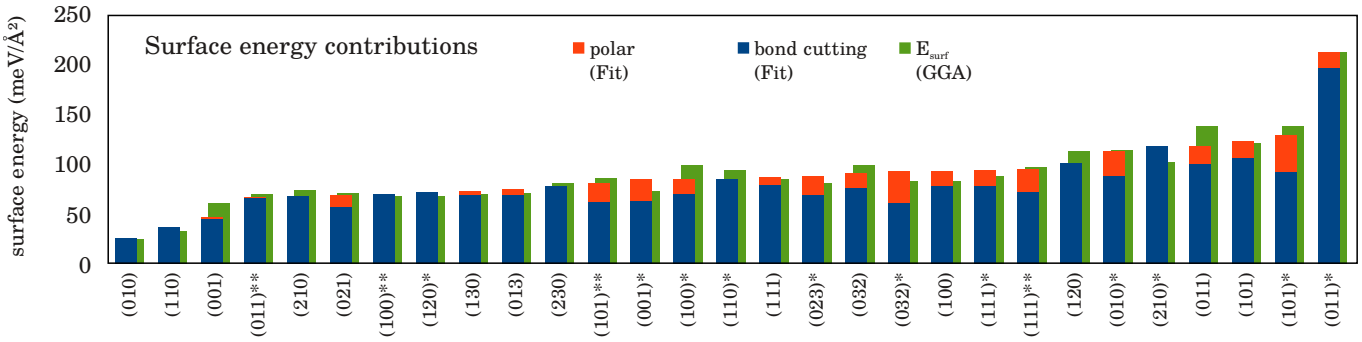

Figure 10. Surface energies of 29 surfaces of $Pmn2_1$ Li_2FeSiO_4. The fitted model allows for a decomposition of *polar* (cost of charge compensation to remove polarity) and bond cutting contributions. Obviously electrostatics plays a minor contribution in total stability. ()* and ()** indicate different terminations for a certain (hkl) surface.

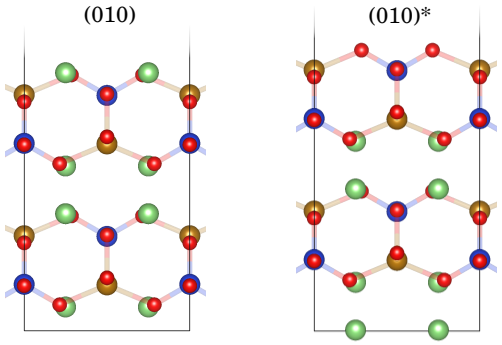

Figure 11. Two possible (010) terminations. The most stable, *non-polar* (010) termination on the left, and the *polar* (010)* termination on the right.

the creation of this surface we speculate that the bond-breaking part of the total surface energy should not differ significantly between GGA and GGA+U calculations, as we do not see significant changes in the Li-O hybridization in the GGA and GGA+U DOS (see Fig. 5a). Accordingly, we find very similar GGA and GGA+U surface energy values for the *non-polar* (010) surface, near the limits of accuracy (table V). As the *polar* (010)* surface also involves only broken Li-O bonds, we assume that the same holds true here (see Fig. 11). Hence we attribute the difference of 24 meV/Å^2 in surface energy between GGA and GGA+U calculations (table V) mainly to changes in the *polar* energy term, due to charge redistribution.

Let us see how this fits into the model: We have seen from the GGA fit that the *polar* energy term K is 0.383 V, and that both (010) surfaces are well-represented by the model (see the surface energies of the (010) and (010)* terminations in Fig. 10). According to our derivation, we conclude that K is proportional to E_g, where we relate E_g to $E_{g1} + E_{g2}$ of the bulk density of states. Therefore we can estimate K = 0.827 V for GGA+U. Thus the *polar* energy part can be estimated to be $0.383 \cdot 0.0636$ eV/Å^2 $\approx$ 24 meV/Å^2 for GGA and to $0.827 \cdot 0.0634$ eV/Å^2 $\approx$ 52 meV/Å^2 for GGA+U. We see the perfect correspondence of the difference in DFT calculation (24 meV/Å^2) with the expected difference from the simple charge redistribution model (28 meV/Å^2) as a further hint that the bond-breaking plus *polar* charge redistribution model indeed captures the important parts for understanding the stability of surfaces, and that the derived polar energy term makes sense.

IV. SUMMARY

We have derived in a consistent way an estimate for the electrostatic part of the surface energy for *polar* surfaces which diverges in the limit of static point charges as in the ionic model. We considered electronic charge redistribution as a compensation mechanism and showed that the converged electrostatic part of the surface energy can be approximated to first order by $\frac{1}{2}\frac{E_g}{e}\sigma_0$, which puts the instability of *polar* surfaces into perspective. E_g is the bandgap or better the energy difference for redistribution of electrons (chemical hardness), which is typically the size of the band gap. Additional correction terms arise due to band filling. We estimated upper boundaries for the surface energy of *polar* surfaces and argued that the effective surface charge σ_0 should be considered as measure for relative stability estimations, and showed that even for the prototypical ZnO (0001) surface no more than one third of the surface energy can be attributed to polarity. Hence a major part must still be attributed to bond cutting, which is why one should not exclude surfaces from our study on Li_2FeSiO_4 [33] based on their

Table V. Surface energies for the *non-polar* and *polar* (010) surface obtained within GGA and GGA+U (U_{eff} = 4 eV). We also show effective surface charges (from oxidation states).

surface	(010) *non-polar*		(010)* *polar*	
method	GGA	GGA+U	GGA	GGA+U
γ_s (meV/Å^2)	24.7	25.4	113.2	137.2
σ_0 (e/Å^2)	0	0	0.0636	0.0634

polar nature.

An important result of the present study is that also *polar* surfaces of complex materials can be understood within a simple ionic model with polarity compensation. The *polar* (001) surface was analyzed as an example, where charge redistribution between Fe atoms was observed, just as expected from the model and the d-d type gap of the bulk DOS. Furthermore the limiting potential drop was found as expected to correspond to the bandgap. We decomposed surface energies into its individual contributions by fitting an energy expression that includes a bond-cutting and a *polar* charge compensation term to surface energies. We tested if our understanding of the surface energy is correct by analyzing the differences obtained in GGA and GGA+U calculations of one *polar* and one *non-polar* (010) termination. Indeed we find very good agreement between model and DFT calculations, which encourages us to apply our surface energy expression to other polymorphs of the same material. It might also be interesting to check the effect of polarity compensation on other materials. It seems very promising to us to look at slabs with a fixed type and number of broken bonds whose dipole can be changed by shuffling atoms from one side to the other. This is possible, e.g., in non-stoichiometric slabs of the *polar* (111) surface in binary rock salt materials (NaCl, MgO). Our method also allows to address the surface structure of further ionic materials that are promising candidates for electrodes in electrochemical energy storage.

V. ACKNOWLEDGMENTS

Generous supply of computer time at the Leibniz Rechenzentrum (LRZ) in Garching is gratefully acknowledged.

[1] J. Goodenough, *J. Solid State Electrochem.*, 2012, **16**, 2019–2029.
[2] N. W. Ashcroft and N. D. Mermin, *Solid State Physics*, Brooks/Cole, third indian reprint ed., 2007.
[3] E. Madelung, *Physikalische Zeitschrift*, 1918, **19**, 542.
[4] P. P. Ewald, *Annalen der Physik*, 1921, **369**, 253–287.
[5] A. Groß, *Theoretical Surface Science - A Microscopic Perspective*, Springer, 2009.
[6] P. W. Tasker, *J. Phys. C: Solid State Phys.*, 1979, **12**, 4977.
[7] F. Bertaut, *Comptes Rendus*, 1958, pp. 3447 – 3450.
[8] R. S. Mulliken, *J. Chem. Phys.*, 1955, **23**, 1833–1840.
[9] T. A. Manz and D. S. Sholl, *J. Chem. Theory Comput.*, 2012, **8**, 2844–2867.
[10] M. Stengel, *Phys. Rev. B*, 2011, **84**, 205432.
[11] C. Noguera, *J. Phys.: Condens. Matter*, 2000, **12**, R367.
[12] A. Wander, F. Schedin, P. Steadman, A. Norris, R. McGrath, T. Turner, G. Thornton, and N. Harrison, *Phys. Rev. Lett.*, 2001, **86**, 3811–3814.
[13] B. Meyer and D. Marx, *Phys. Rev. B*, 2003, **67**, 035403.
[14] D. Wolf, *Phys. Rev. Lett.*, 1992, **68**, 3315–3318.
[15] P. A. Mulheran, *Modell. Simul. Mater. Sci. Eng.*, 1994, **2**, 1123.
[16] A. Eichler and G. Kresse, *Phys. Rev. B*, 2004, **69**, 045402.
[17] G. Kresse, O. Dulub, and U. Diebold, *Phys. Rev. B*, 2003, **68**, 245409.
[18] F. Finocchi, A. Barbier, J. Jupille, and C. Noguera, *Phys. Rev. Lett.*, 2004, **92**, 136101.
[19] A. Wander, I. J. Bush, and N. M. Harrison, *Phys. Rev. B*, 2003, **68**, 233405.
[20] C. Noguera and J. Goniakowski, *J. Phys.: Condens. Matter*, 2008, **20**, 264003.
[21] J. Goniakowski, F. Finocchi, and C. Noguera, *Rep. Prog. Phys.*, 2008, **71**, 016501.
[22] J. Goniakowski, C. Noguera, and L. Giordano, *Phys. Rev. Lett.*, 2007, **98**, 205701.
[23] A. Groß, *Surf. Sci.*, 2002, **500**, 347.
[24] G. Ceder, *MRS Bulletin*, 2010, **35**, 693–702.
[25] G. Zhong, Y. Li, P. Yan, Z. Liu, M. Xie, and H. Lin, *J. Phys. Chem. C*, 2010, **114**, 3693–3700.
[26] L. Bao, W. Gao, Y. Su, Z. Wang, N. Li, S. Chen, and F. Wu, *Chin. Sci. Bull.*, 2012, 1–10.
[27] R. Dominko, M. Bele, M. Gaberscek, A. Meden, M. Remskar, and J. Jamnik, *Electrochem. Commun.*, 2006, **8**, 217–222.
[28] M. Arroyo-deDompablo, R. Dominko, J. Gallardo-Amores, L. Dupont, G. Mali, H. Ehrenberg, J. Jamnik, and E. Moran, *Chem. Mater.*, 2008, **20**(17), 5574–5584.
[29] M. Arroyo y de Dompablo, J. Gallardo-Amores, J. García-Martínez, E. Morán, J.-M. Tarascon, and M. Armand, *Solid State Ionics*, 2008, **179**, 1758–1762.
[30] S.-I. Nishimura, S. Hayase, R. Kanno, M. Yashima, N. Nakayama, and A. Yamada, *J. Am. Chem. Soc.*, 2008, **130**, 13212.
[31] C. Sirisopanaporn, C. Masquelier, P. G. Bruce, A. R. Armstrong, and R. Dominko, *J. Am. Chem. Soc.*, 2011, **133**, 1263–1265.
[32] A. Nyten, S. Kamali, L. Haggstrom, T. Gustafsson, and J. O. Thomas, *J. Mater. Chem.*, 2006, **16**, 2266–2272.
[33] N. Hörmann and A. Groß, *J. Solid State Electrochem., doi: 10.1007/s10008-013-2189-x*, 2014.
[34] L. A. Mancera, R. J. Behm, and A. Groß, *Phys. Chem. Chem. Phys.*, 2013, **15**, 1497–1508.
[35] A. Calzolari, M. Bazzani, and A. Catellani, *Surf. Sci.*, 2013, **607**, 181 – 186.
[36] J. D. Jackson, *Classical Electrodynamics Third Edition*, Wiley, third ed., 1998.
[37] W. W. Lee and S.-I. Choi, *J. Chem. Phys.*, 1980, **72**, 6164.
[38] G. Kresse and J. Furthmüller, *Phys. Rev. B*, 1996, **54**, 11169–11186.
[39] G. Kresse and J. Furthmüller, *Comput. Mater. Sci.*, 1996, **6**, 15 – 50.
[40] J. P. Perdew, K. Burke, and Y. Wang, *Phys. Rev. B*, 1996, **54**, 16533–16539.
[41] S. L. Dudarev, G. A. Botton, S. Y. Savrasov, C. J. Humphreys, and A. P. Sutton, *Phys. Rev. B*, 1998, **57**,

1505–1509.
[42] F. Zhou, M. Cococcioni, C. A. Marianetti, D. Morgan, and G. Ceder, *Phys. Rev. B*, 2004, **70**, 235121.
[43] M. Arroyo-de Dompablo, M. Armand, J. Tarascon, and U. Amador, *Electrochem. Commun.*, 2006, **8**, 1292–1298.
[44] A. Saracibar, A. Van der Ven, and M. E. Arroyo-de Dompablo, *Chem. Mater.*, 2012, **24**, 495–503.
[45] L. Wang, T. Maxisch, and G. Ceder, *Phys. Rev. B*, 2006, **73**, 195107.
[46] S. Wu, Z. Zhu, Y. Yang, and Z. Hou, *Comput. Mater. Sci.*, 2009, **44**, 1243 – 1251.
[47] C. Eames, A. R. Armstrong, P. G. Bruce, and M. S. Islam, *Chem. Mater.*, 2012, **24**, 2155–2161.
[48] J. Zaanen, G. A. Sawatzky, and J. W. Allen, *Phys. Rev. Lett.*, 1985, **55**, 418–421.
[49] J. Zaanen, G. Sawatzky, and J. Allen, *J. Magn. Magn. Mater.*, 1986, **54**, 607 – 611.
[50] J. Zaanen and G. Sawatzky, *J. Solid State Chem.*, 1990, **88**, 8 – 27.
[51] G. Henkelman, A. Arnaldsson, and H. Jonsson, *Comput. Mater. Sci.*, 2006, **36**, 354 – 360.

Table of content entry:

Polar surfaces: An expression is derived that describes the effect of electron transfer between two exposed polar surfaces due to the internal electric field generated by the surfaces and applied to Li_2FeSiO_4 which is interesting as possible electrode material of future Li-ion batteries.